Ammonia synthesis on $BaTiO_{2.5}H_{0.5}$: Computational insights into role of hydrides

Kristen Wang,[a] Zili Wu,[b,c] and De-en Jiang*[a]

[a]Department of Chemistry, University of California, Riverside, CA 92521, USA

[b]Chemical Sciences Division, Oak Ridge National Laboratory, Oak Ridge, Tennessee 37831, United States

[c]Center for Nanophase Materials Sciences, Oak Ridge National Laboratory, Oak Ridge, Tennessee 37831, United States

*To whom correspondence should be addressed. E-mail: djiang@ucr.edu

Abstract

Perovskite oxyhydrides such as $BaTiO_{2.5}H_{0.5}$ have been found to be able to catalyze NH_3 synthesis, but the mechanism and the role of the catalyst's lattice hydrides in the catalytic reaction remain unknown. Here we employ first principles density functional theory to investigate the mechanism of ammonia synthesis and the role of lattice hydrides on a prototypical perovskite oxyhydride, $BaTiO_{2.5}H_{0.5}$. Two mechanistic hypotheses, the distal and alternating pathways, have been tested on the Ti_2O_2 termination of the BTOH (210) surface, previously determined to be the most stable surface termination at the reaction conditions considered. In the distal pathway, H atoms hydrogenate N_2 to form the *N-NH_x key intermediates, followed by N-N bond breaking. In the alternating pathway, H atoms hydrogenate N_2 in an alternating fashion to form the *NH_x-NH_y intermediates before N-N bond breaking and formation of co-adsorbed *NH_x/*NH_y on the surface. We find that the subsurface hydride vacancy formed after reaction of *N_2 with the lattice hydride is key to the distal pathway, leading to surface nitride formation after breaking the *N-NH_3 bond, while the neighboring surface Ti sites are key to bridging and stabilizing the *NNH intermediate in the alternating pathway. In both pathways, desorption of NH_3 is the most uphill process in energy. Our results provide important insights into the role of hydrides and surface vacancies in hydrogenation reactions over BTOH that will be useful to guide future spectroscopic experiments such as operando IR and inelastic neutron scattering to verify the key intermediates.

1. Introduction

Complex oxides, comprised of at least two metallic elements, find wide applications in thermal catalysis,[1] electrocatalysis,[2] and photocatalysis.[3] Their surfaces can take on numerous configurations and expose different combinations of metal cations and anions, thus providing a myriad of local chemical environments more diverse than binary oxides. For example, when the ABO_3-type perovskite, $LaNiO_3$, is used as the catalyst in CO_2 hydrogenation, CO_2 is selectively converted into CH_4.[4] However, when La cations are partially replaced by K cations, the reaction selectivity shifts from CO_2 methanation to the reverse water gas shift (rWGS) reaction. The incorporation of K promotes the formation of thermally unstable C-intermediates that escape hydrogenation to form the rWGS reaction products rather than CH_4 from CO_2 methanation.[4]

The catalytic properties of complex oxides can also be tuned by anion substitution such as in the case of perovskite oxyhydrides ($ABO_{3-x}H_x$). These mixed-anion perovskite materials are the hydride-reduced forms of the ABO_3 perovskites where lattice O^{2-} are randomly replaced by H^- to form the mixed-anion material.[5,6,7] Previously, there have been very few well-characterized oxyhydride compounds; the first mixed oxyhydride was discovered in 1982 with the synthesis of LaHO.[8] This material was found to be highly hygroscopic and releases hydrogen when in contact with ambient moisture. Later on, other oxyhydride materials such as $Ba_3(AlO_4)H$ [9] and $Ba_{21}Ge_2O_5H_{24}$[10] were synthesized, albeit under extremely reducing conditions. It was not until 2002 when Hayward *et al.* showed how the $LaSrCoO_4$ layered-perovskite's structure can be preserved upon reacting with CaH_2 to form the $LaSrCoO_3H_{0.7}$ oxyhydride using a soft chemistry method.[11] These earlier works paved the way to the discovery of an air and water-stable barium titanium oxyhydride in 2012 by Kobayashi *et al.*[5] Since then, a vast number of other types of perovskite oxyhydrides have been synthesized which contain other elements such as Sc,[12] V,[13,14] Cr,[15] or Mn[16] as the B-cation.

Catalysis over perovskite oxyhydride solids have lately been of interest due to the impact lattice hydrides have on the oxyhydride's redox properties and electronic structure. For example, using the $BaTiO_{3-x}H_x$ perovskite oxyhydride as a support results in an enhanced catalytic activity in hydrogenation reactions including CO_2 methanation and ammonia synthesis.[17,18] This observed improvement in reaction rate was attributed to the following factors: (i) the material's labile hydrides providing a spillover pathway for the incoming H_2, thus preventing the Ru metal catalyst

from being poisoned; (ii) the participation of lattice hydrides in the catalytic cycle via a hydride-based Mars-van Krevelen (MvK) mechanism; (iii) the transfer of charges to the metal centers which assists in N_2 activation.[17,18] Furthermore, $BaTiO_{3-x}H_x$ (with x = 0.5) alone is also active for ammonia synthesis under conditions (i.e. 400 ^oC, 5MPa) comparable to the Haber-Bosch conditions over an iron-based catalyst.[19,31] But the role of lattice hydrides in ammonia synthesis over $BaTiO_{2.5}H_{0.5}$ has been unclear.

Perovskite oxyhydrides can further incorporate nitride ions because their labile hydrides [5,6,7,20,21] can easily desorb as H_2[5,6] or exchange with nitrogen anions or halides starting at a temperature of 673 K.[22] This property further enriched their catalytic capability. For instance, the $BaCeO_{3-x}N_yH_z$ perovskite oxynitride-hydride was shown to be able to incorporate its lattice nitrogen and hydrogen species in the synthesis of ammonia and subsequently replace those lattice sites by gas-phase nitrogen or hydrogen via an anion-vacancy mediated Mars-van Krevelen mechanism.[23]

The emergence of perovskite oxyhydrides as a new class of mixed-anion materials for catalysis necessitates fundamental understandings of their surface structure and the corresponding structure-activity-selectivity relationships for catalysis. Building off our previous study on the stable surface terminations of $BaTiO_{2.5}H_{0.5}$,[30] here we aim to reveal the role of lattice hydrides in $BaTiO_{2.5}H_{0.5}$ (BTOH) for ammonia synthesis from N_2 and H_2. This work will also lay a foundation for future studies of BTOH as a support for metal catalysts. Below, we first introduce the computational methods and our surface model.

2. Computational Methods

Spin-polarized density functional theory (DFT) calculations were performed using the Vienna *ab initio* Simulation Package (VASP).[24,25] Electron exchange and correlation energies were treated at the general-gradient approximation (GGA) level using the Perdew-Burke-Ernzerhof (PBE) functional[26] and the electron-core interactions were described by the projector augmented-wave (PAW) potentials.[27] The electronic wave functions were expanded using a plane wave basis set with kinetic cutoff energy of 450 eV and the van der Waals interactions were

accounted for by DFT-D3.[28] The convergence criteria for force and energy were 0.02 eV/Å and 10^{-5} eV, respectively. Bader charge analysis was used to obtain the partial atomic charges.[29]

The same BTOH double-cubic, tetragonal unit cell from our previous study[30] was used and has lattice parameters of a = 8.06 Å, b = c = 4.03 Å. The BTOH (210)-Ti_2O_2 surface termination, previously determined to be the most stable termination[30] under the NH_3 synthesis conditions[31] via first principles thermodynamics applied to perovskite surfaces,[32] was used as a model structure for mechanistic studies. Here we note that, because we used the double-cubic cell for our bulk BTOH structure, the (210) surface of our unit cell resembles the (110) surface of a cubic unit cell of $BaTiO_3$. The bottom three layers of the six-layered slab for the BTOH (210)-Ti_2O_2 surface were fixed in their bulk positions and a 3×3×1 k-point mesh in the Monkhorst-Pack scheme[33] was used to sample its Brillouin zone. To compensate the net dipole moment along the surface normal due to slab asymmetry, a dipole correction[34] was included within the vacuum region.

Adsorption energies were calculated according to the equation

$$E_{ads} = E_{surface+adsorbate} - (E_{surface} + E_{adsorbate}) \quad (1)$$

where $E_{surface+adsorbate}$, $E_{surface}$, and $E_{adsorbate}$ are the electronic energies for the adsorbate-slab system (adsorbates are either a reactant, intermediate, or product), the clean surface, and the isolated adsorbate molecules (H_2, N_2, or NH_3), respectively. The energies of N_2, H_2, and NH_3 were computed by placing each adsorbate in a 15×15×15 $Å^3$ cell. The climbing-image nudged elastic band (CI-NEB) method[35] was used to search the transition state for H_2 dissociation over the BTOH surface; the force convergence criterion was set to 0.05 eV/ Å and the transition state found was verified by vibrational frequency analysis.

The change in Gibbs free energy corresponding to NH_3 desorption (ΔG_{des}) from the surface was approximated using the following equation

$$\Delta G_{des} = \Delta H_{des} - T\Delta S_{des} \approx (\Delta E_{elec} + \Delta E_{vib}) - T\Delta S_{des} \quad (2)$$

where ΔE_{elec} is the change in electronic energy, ΔE_{vib} is the change in vibrational energy, T is temperature at 673 K, and ΔS_{des} is the change in entropy between the adsorbed state (initial state) and the desorbed state (final state). The finite-difference method, as implemented in VASP, was used to compute the vibrational frequencies of isolated NH_3 as well as NH_3 adsorbed on a

completely fixed slab. In this work, the desorption energy of NH_3 from the BTOH surface is >1 eV when calculated using only electronic energies. The purpose of calculating the Gibbs free energy of desorption here is to qualitatively show that NH_3 desorption from the BTOH surface is much lower than 1 eV. Therefore, we approximate the rotational and vibrational entropic contributions to be less than the translational entropic contribution and

$$\Delta S_{des} = S_{NH_3} - S_{NH_3{}^*} = S_{NH_3} - \left(S_{NH_3} - S_{NH_3,trans}\right) = S_{NH_3,trans} \quad (3)$$

where S_{NH3} is the total entropy of gaseous NH_3, S_{NH3*} is the total entropy of adsorbed NH_3, and $S_{NH3,trans}$ is the translational entropy of gaseous NH_3. The Sackur-Tetrode equation was used to calculate the translational entropy of NH_3 in the gaseous state.[36] Section 1 of the Supporting Information (ESI) lists the equations used to calculate $S_{NH3,\,trans}$ and ΔG_{des}.

3. Results and Discussion

The key steps of NH_3 synthesis include N_2 adsorption and activation, H_2 adsorption and activation, and NH_3 formation and desorption. Because of the complication and complexity from the expected participation of lattice hydrides in the reaction, our mechanistic studies will especially focus on the role of hydrides and hydrogenation steps. We start with an analysis of the surface structure of the BTOH (210)-Ti_2O_2 termination.

3.1 Surface structure of BTOH (210)-Ti_2O_2 surface termination

We previously found[30] that the most stable BTOH surface termination under NH_3 synthesis conditions (673 K and under 5 MPa of pressure)[31] is (210)-Ti_2O_2. A side view of the 2×2 slab model and of the top two layers are shown in Fig. 1. This vicinal surface has a corrugated surface structure with each of the two ridges consisting of TiO (Fig. 1b), hence the Ti_2O_2 name. The 2×2 supercell exposes four surface Ti and four surface O atoms. Ti^A and Ti^B have an average Bader charge of +1.84 |e|, each bonded to two subsurface O atoms; Ti^C and Ti^D are slightly more reduced and have an average Bader charge of +1.71 |e|, each bonded to one subsurface O and one subsurface H atom (Fig. 1b). The bond lengths between surface and subsurface atoms of the BTOH (210)-Ti_2O_2 surface are shown in Fig. S1. The two different types of Ti atoms on the surface are a result of an electron donation into the Ti 3d conduction bands when O^{2-} is substituted by H^- during

the hydride reduction of $BaTiO_3$.[7, 37] It is expected that the two different types of surface Ti will have different reactivity toward reactants, which is examined next.

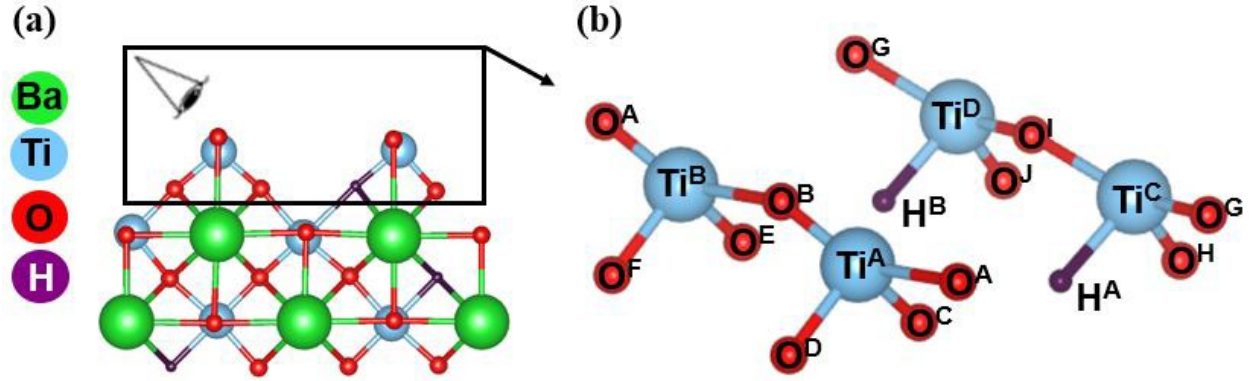

Fig. 1. Structure model of the (210)-Ti_2O_2 surface of $BaTiO_{2.5}H_{0.5}$: (a) side view of the slab; (b) perspective view of the top two layers showing various Ti, O, and H sites.

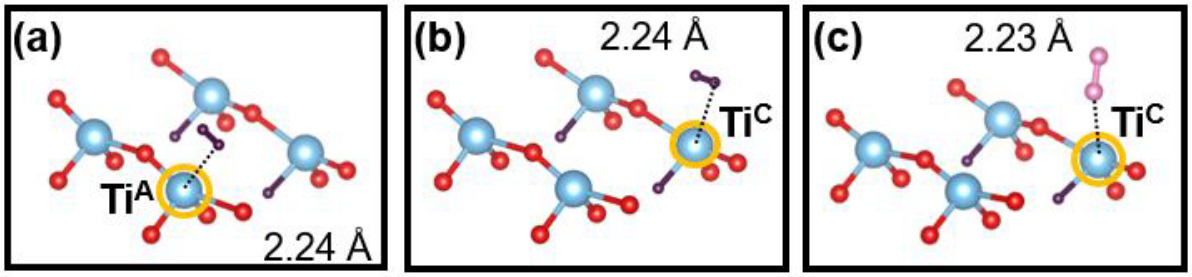

Fig. 2. The most stable adsorption structures for H_2 (a and b) and N_2 (c) on the (210)-Ti_2O_2 surface of $BaTiO_{2.5}H_{0.5}$. Shown also are the distances (dashed lines) between the adsorbate and the nearest surface atom (circled in yellow and labeled). Color code: blue, Ti; red, O; pink, N; purple, H.

Table 1. Adsorption energies (E_{ads}) of N_2 and H_2 on the different surface sites of BTOH (210)-Ti_2O_2.

Adsorbate	**Surface Site**	**E_{ads} (eV)**	**Adsorbate**	**Surface Site**	**E_{ads} (eV)**
N_2	Ti^A	-0.31	H_2	O^A	-0.08
N_2	Ti^C	-0.42	H_2	O^B	-0.08
H_2	Ti^A	-0.22	H_2	O^G	-0.07
H_2	Ti^C	-0.22	H_2	O^I	-0.06

3.2 Adsorption of reactants on BTOH (210)-Ti_2O_2 surface

The adsorption positions of the N_2 and H_2 molecules on BTOH were first determined prior to exploring ammonia synthesis pathways over the catalytic surface. To fully consider all possible adsorption sites, N_2 and H_2 were adsorbed at surface sites of different coordination environments (Fig. 1b) and the corresponding adsorption energies are reported in Table 1, while the most stable adsorption structures of each molecule are shown in Fig. 2. One can see that H_2 preferably adsorbs onto a surface Ti than an O site, with no selectivity for Ti^A or Ti^C, and adopts a tilted geometry with one H atom closer to the Ti atom (Fig. 2a, b). The same adsorption energy of H_2 on the two different Ti sites can be attributed to the physical nature of the adsorption which is less sensitive to the chemical difference between the two Ti sites.

N_2 activation typically occurs when the molecule's filled σ-orbital bonds with the metal's d_{z2} or d_{x2-y2} orbitals and the electrons in the metal's d_{xz}, d_{yz}, or d_{xy} orbitals back-donate into the vacant π*-orbital of N_2.[38] Hence, we considered only the Ti sites. We found that N_2 molecule prefers to adsorb terminally (Fig. 2c) on the more reduced Ti^C atom than on Ti^A (Table 1). The local density of states (DOS) as a result of the interaction between the N_2 molecule with Ti^A or Ti^C is shown in Fig. 3. One can see greater orbital hybridization between N_2 and Ti^C than between N_2 and Ti^A. The charge-density difference plot and the Bader charges of N (Fig. 3c) clearly show charge accumulation along the Ti-N bonding region, depleted from Ti and the far-end N atom.

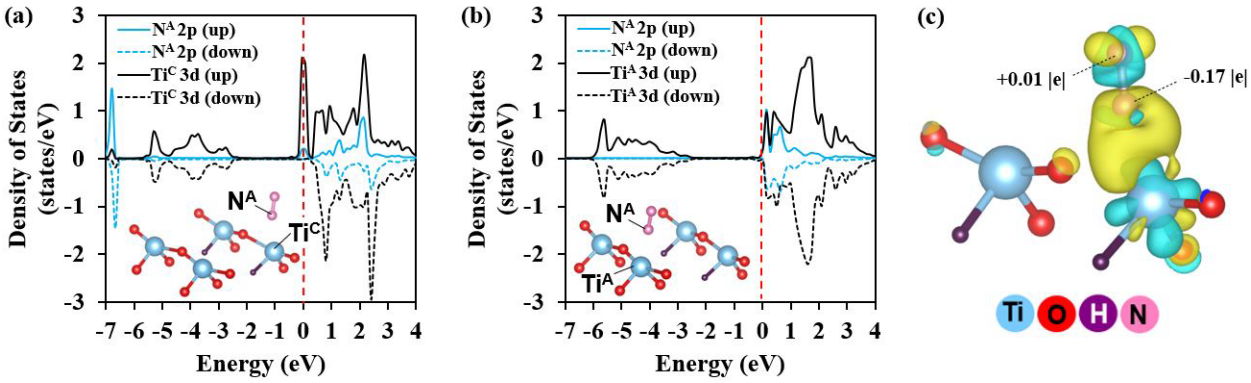

Fig. 3. The local density of states of N_2 adsorbed BTOH (210)-Ti_2O_2: (a) on Ti^C; (b) on Ti^A. (c) Charge-density-difference plot of the N_2-Ti^C configuration: the yellow region represents charge accumulation, and the blue region charge depletion; the Bader charges on each N atom are also shown.

3.3 Reaction mechanisms of ammonia synthesis on the BTOH (210)-Ti_2O_2 surface

During NH_3 synthesis, BTOH lattice hydrides can incorporate into the catalytic cycle. A previous study has shown this direct involvement of the mobile lattice hydrides for NH_3 synthesis when deuterated NH_3 was initially produced over the $Ru/BaTiO_{2.4}D_{0.6}$ catalyst.[18] On the other hand, we found that H_2 readily dissociates across the surface Ti-O bond, as indicated by the relatively low barrier of 0.15 eV (Fig. S3), thereby replenishing the surface H atoms used to hydrogenate N_2 to NH_3. Here we considered two likely pathways for ammonia synthesis on the (210)-Ti_2O_2 surface termination of BTOH. Both pathways proceed first with H_2 adsorption and dissociation on the surface and then reduction of N_2 by either H_2-sourced surface H atoms or surface lattice hydrides followed by N-N cleavage. Fig. 4 shows the mechanistic overview of the two pathways studied: (a) the distal pathway whereby H atoms hydrogenate N_2 to form the *N-NH_2 and *N-NH_3 key intermediates, followed by N-N bond breaking; (b) the alternating pathway whereby H atoms hydrogenate N_2 in an alternating fashion to form the intermediates such as *NHNH, before N-N bond breaking, and formation of co-adsorbed *NH/*NH_2 and *NH_2/*NH_2 on the surface. The pathway starting with N_2 dissociation prior to H addition was not pursued because we found that dissociation of N_2 into two N atoms adsorbed on surface Ti sites is a highly uphill process (> 6 eV; see Fig. S4 in ESI). Below we examine the two pathways in detail.

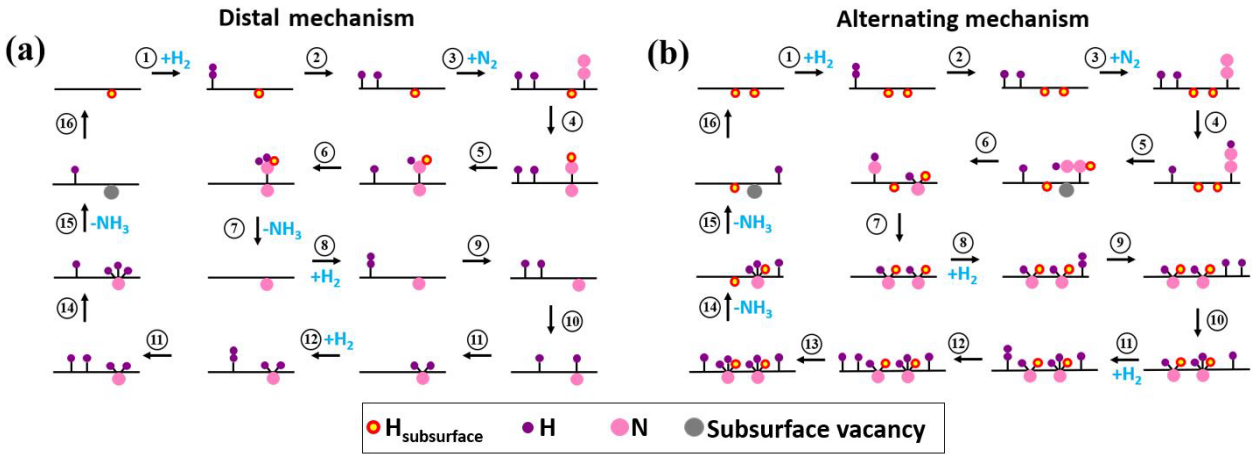

Fig. 4. A mechanistic overview of (a) the distal and (b) alternating mechanisms for NH_3 synthesis over BTOH. The BTOH surface is represented as a horizontal black line and any atom below the line represent subsurface atoms. The gray dot represents a subsurface vacancy.

3.3.1 The distal pathway

Fig. 5a shows the energy profile of the key states involved in the formation of the two NH_3 molecules and Fig. 5b shows the structures of the key intermediates on the surface. Formation of the first NH_3 molecule starts with H_2 adsorption and then dissociation across the surface Ti^C-O^I bond (states 1 to 3). After N_2 adsorption on Ti^C (state 4), a surface lattice hydride hydrogenates $*N_2$ to *NNH (state 5) which subsequently moves to the hydride-vacancy site occupied previously by the subsurface lattice hydride (structure 5 in Fig. 5b). We found that this configuration is more stable than the one where the hydride from H_2 dissociation hydrogenates N_2 while the surface lattice hydride stays in place (Fig. S5 in ESI). In this configuration, the N-N bond length elongates to 1.30 Å from 1.11 Å in the gas phase N_2. From there, the two surface H atoms from H_2 consecutively hydrogenate *NNH to form $*NNH_2$ (state 6) and then $*NNH_3$ (state 7). Next, the N-N bond is cleaved, leaving a subsurface lattice nitride and an NH_3 molecule adsorbed on Ti^C (state 8). Local density-of-states (DOS) plots (Fig. 6) show that state 8 has greater orbital hybridization between N 2p and Ti 3d than state 7, suggesting that state 8's much lower energy is contributed by both formation of a stable molecule (NH_3) and the stronger Ti-N interaction. Although it requires 1.5 eV in energy to desorb the NH_3 molecule from state 8, the free energy of NH_3 desorption is significantly lower at 0.28 eV after adding the favorable entropy contribution due to formation of a gaseous NH_3 molecule (state 9) at the reaction temperature.

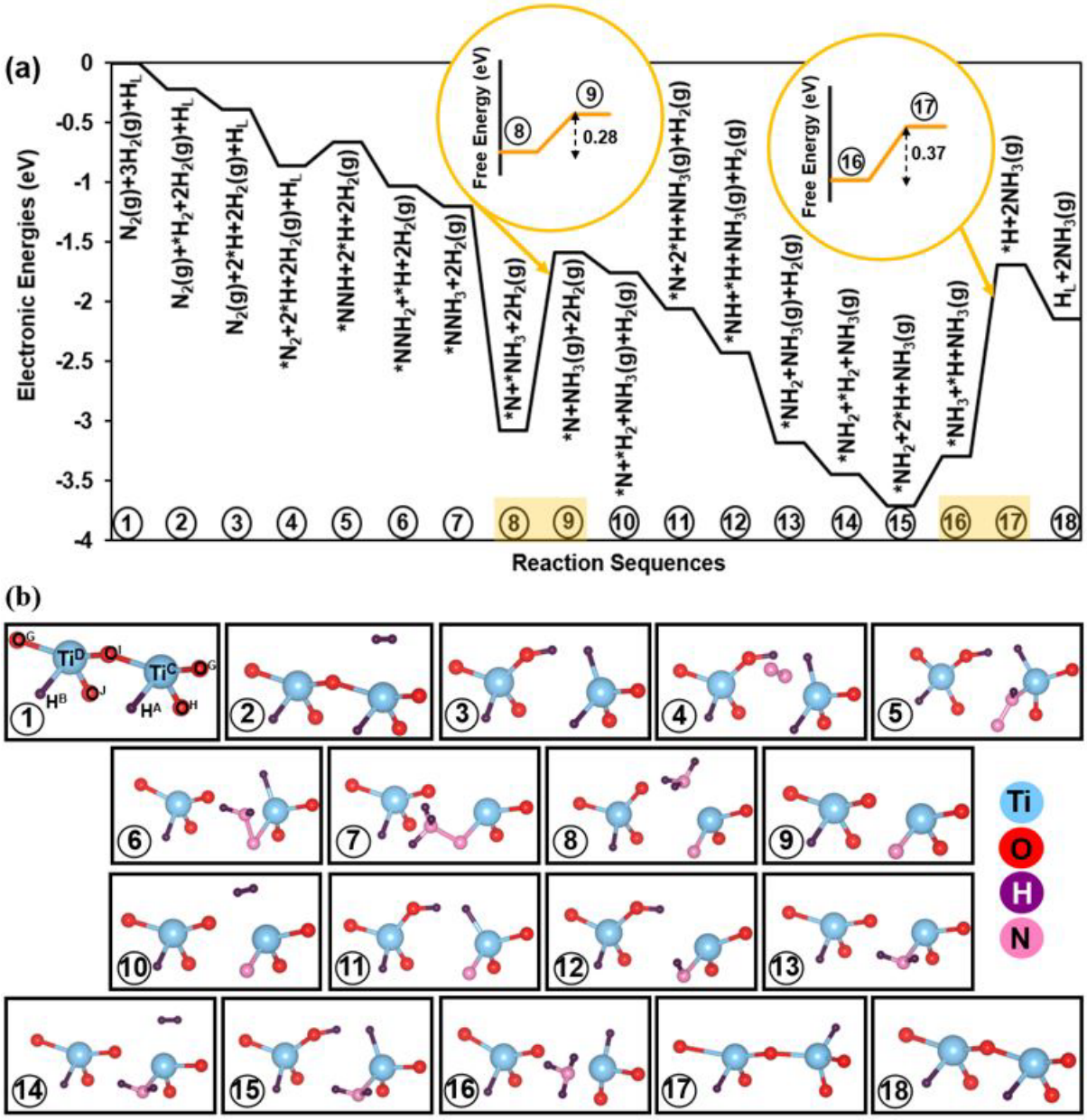

Fig. 5. Formation of the two NH_3 molecules via the distal mechanism. Gaseous and adsorbed states are represented by (g) and *, respectively. The free energy of desorption of the 1st and 2nd NH_3 molecules (ie. 0.28 and 0.37 eV, respectively) are shown in the orange bubble in (a). All intermediate structures are modeled in (b).

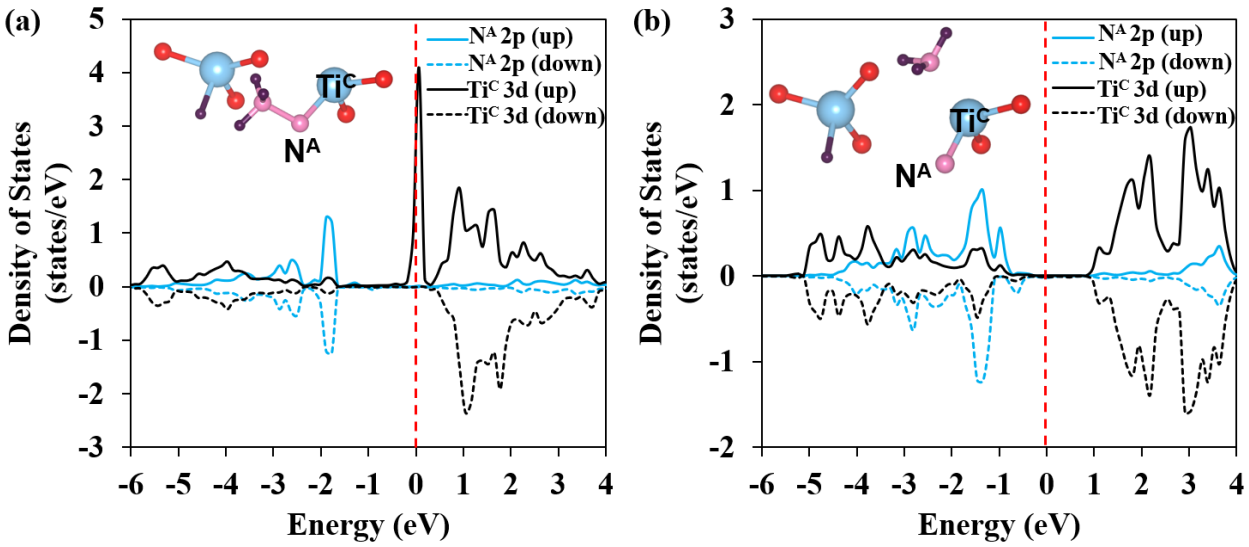

Fig. 6. Local density of states (DOS) of state 7 (a) and state 8 (b) in the distal pathway.

In states 10-18, a second NH_3 molecule is formed by hydrogenating the subsurface lattice nitride in state 9 with three more surface H's from the dissociation of two H_2 molecules, while the fourth H atom is used to regenerate the surface lattice hydride site. The second adsorbed H_2 molecule is heterolytically cleaved across Ti^C and O^I (states 10-11). Next, H on Ti^C transfers to *N to form *NH (state 12) which is further hydrogenated to *NH_2 (state 13) by H on O^I. Then the third H_2 molecule adsorbs (state 14) and heterolytically cleaves across Ti^C and O^I atoms (state 15). Further, H on O^I reacts with *NH_2 to form *NH_3 (state 16) with an uphill in energy of 0.41 eV. The second NH_3 desorbs (state 17: ΔE=1.61 eV; ΔG=0.37 eV). Finally, the remaining H adsorbed on Ti^C rotates and fills the subsurface anion vacancy to regenerate the catalytic surface in state 18. Overall, two key factors are involved in the distal pathway: (i) the presence of surface Ti^C and O^I atoms to heterolytically cleave H_2 and generate surface H atoms that hydrogenate *N_2; (ii) the hydride vacancy site to anchor N-NH after the hydride transfers to adsorbed N_2.

3.3.2 The alternating pathway

In this mechanism, both N atoms of N_2 are hydrogenated before N-N bond breaking. Fig. 7 shows the energy profile and structures of key intermediates. The reaction starts with dissociative H_2 adsorption, followed by N_2 adsorption (states 1-4, same as in the distal pathway). The next step is different: instead of subsurface lattice hydride attacking N_2 as in the distal pathway, now the

surface H atom bonded to Ti^C from H_2 dissociation first reacts with $*N_2$ to form *NNH (state 5). The *NNH intermediate is stabilized by bridging Ti^C and Ti^D sites (5 in Fig. 7b). This is an important intermediate in the alternating pathway. Then, one of the subsurface lattice hydrides, H^A, hydrogenates the proximal N of *NNH to form the *NHNH species (state 6), still bridged by Ti^C and Ti^D. Next, the surface H bonded to O^I from H_2 dissociation transfers to *NHNH, leading to cleavage of the N-N bond and formation of co-adsorbed $*NH_2$ at the hydride-vacancy site and *NH on Ti^D (state 7). Subsequent addition of another subsurface lattice hydride, H^B, to *NH results in two $*NH_2$ groups occupying two subsurface hydride-vacancy sites (state 8).

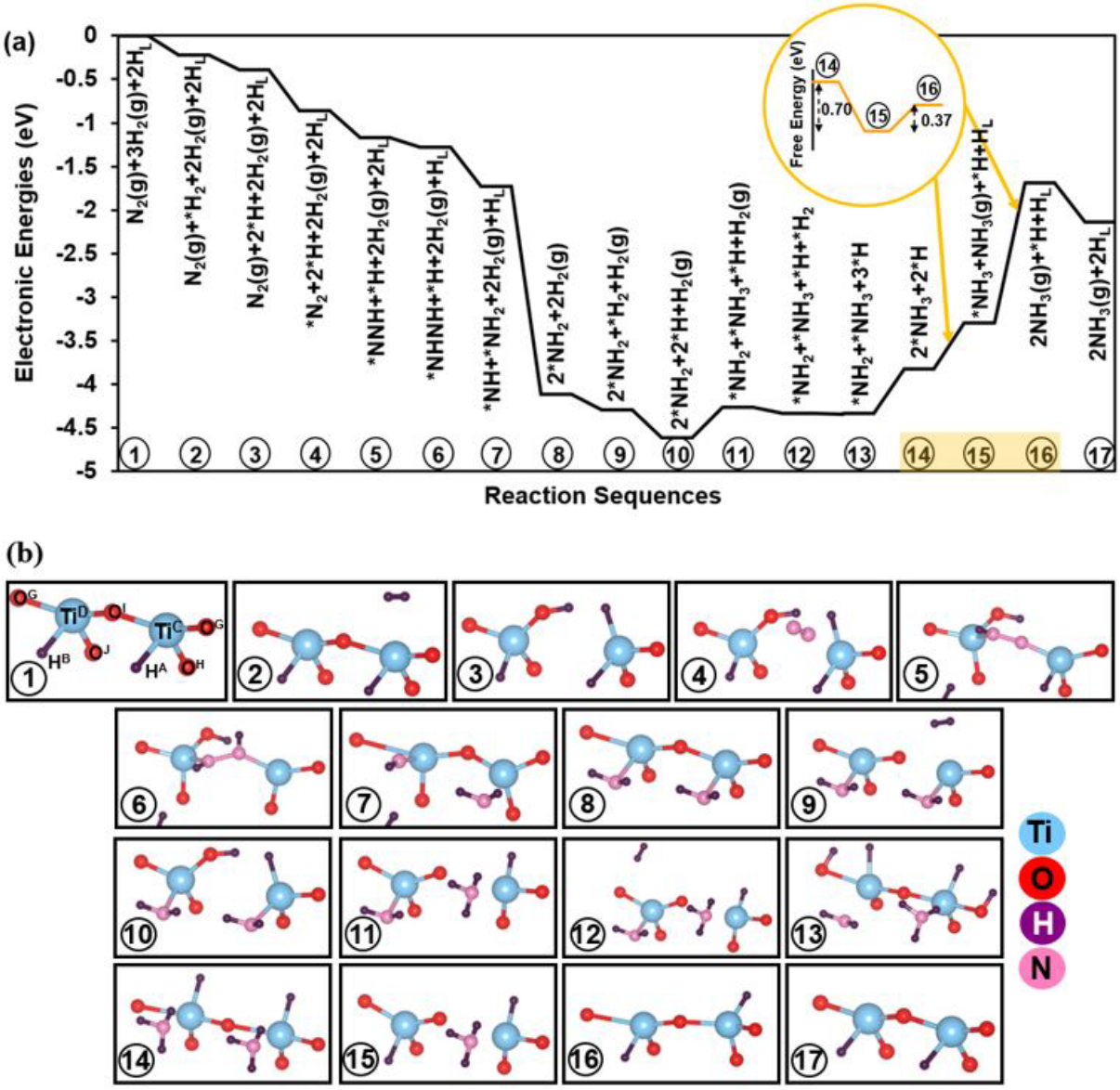

Fig. 7. Formation of the two NH_3 molecules via the alternating mechanism (a). Gaseous and adsorbed states are represented by (g) and *, respectively. The free energy of desorption of the 1st and 2nd NH_3 molecules (ie. -0.70 and 0.37 eV, respectively) are shown in the orange bubble in (a). All intermediate structures are modelled in (b).

Fig. 7a shows that all the states (1 to 8) of N_2 reaction with two lattice hydrides and one molecule of dissociated H_2 to form 2 *NH_2 are downhill, especially from 7 to 8. To understand the origin of this extra stability at state 8, we analyzed in detail the change in the local geometry from 7 to 8 (Fig. 8). One distinct change is the Ti-O distances, especially the distances to the subsurface O atoms shortened from 1.90 and 1.85 Å in Fig. 8a to 1.78 and 1.79 Å in Fig. 8b, respectively. In other words, after hydrogenation of *NH by the subsurface lattice hydride H^B to form two *NH_2 groups occupying two subsurface hydride-vacancy sites, the local bonding of the two surface Ti atoms is greatly strengthened, leading to a much more stable state.

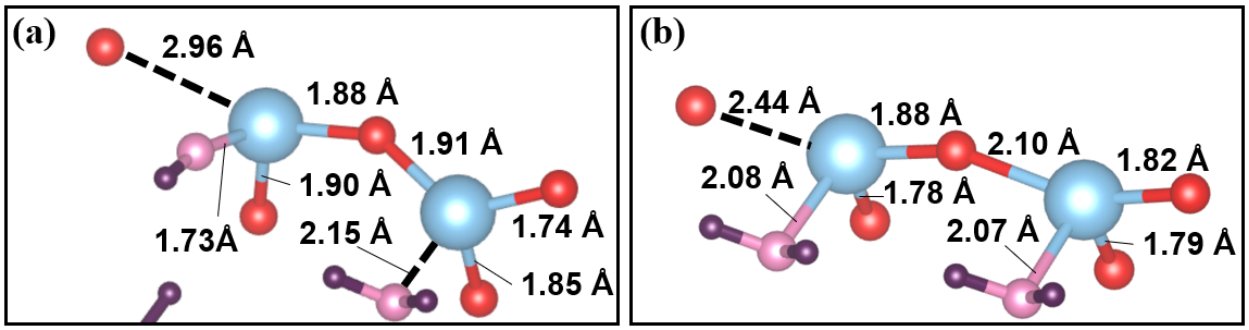

Fig. 8. Local geometry in state 7 (a) and state 8 (b) of the alternating pathway.

In the subsequent states (9 to 17), two more molecules of H_2 adsorb and dissociate on the surface, generating four surface H atoms: two of them hydrogenate NH_2 to NH_3 while the other two regenerate the subsurface lattice hydrides. First, the second H_2 molecule adsorbs (state 9) and dissociates across the surface Ti^C-O^I bond (state 10) to replenish surface H atoms. Then, the surface H on the O^I site hydrogenates one *NH_2 to *NH_3 (state 11; slightly uphill by 0.36 eV). Next, dissociative adsorption of the third H_2 molecule takes place (states 12 and 13). Further, the surface H on the O^G site hydrogenates the remaining *NH_2 to *NH_3 (state 14; uphill by 0.49 eV). The desorption of the first NH_3 molecule happens simultaneously with the H on Ti^D rotating to the

subsurface hydride-vacancy site (state 15: ΔE=0.52 eV; ΔG=-0.70 eV). The desorption of the second NH_3 molecule is significantly more uphill (state 16, ΔE=1.61 eV; ΔG=0.37 eV). Lastly, the remaining hydride adsorbed on Ti^C fills the subsurface vacancy in state 17.

3.3.3 Comparison of the two pathways

In comparing the distal and the alternating pathways, one can see that the crucial bifurcating point is how the first H atom is added to $*N_2$ to form *NNH: in the distal pathway, the first H is a subsurface lattice hydride and after hydrogenation, the proximal N of *NNH is anchored at the anion-vacancy site; in the alternating pathway, the first H is from H_2 dissociation and the *NNH intermediate is bridged between two surface Ti sites. The two different sites for *NNH dictate the two subsequently different paths for N-N cleavage. In the distal pathway, the state of $*NNH_3$ dissociating to *N and $*NH_3$ is most exothermic, while in the alternating pathway it is the hydrogenating of *NH to $*NH_2$. In both pathways, desorption of the NH_3 molecules is the most energetically uphill, especially the second one; but with the entropy gain in forming gaseous NH_3, the free-energy change is much less positive and can even turn negative in the case of the first NH_3 desorption in the alternative pathway. As the distal pathway involves only one hydride/vacancy in the synthesis of ammonia while the alternating pathway involves two adjacent hydrides/vacancies, it suggests that the distal pathway is more likely to happen on $BaTiO_{3-x}H_x$ for smaller x-values while the alternating pathway for larger x values.

3.4 Experimental implications

As Ti is an early transition metal, it bonds strongly with N, making metallic Ti unsuitable for catalytic ammonia synthesis since an inactive surface nitride would be formed from dissociative N_2 adsorption. However, Kobayashi et al. has shown that powdered samples of BTOH exhibited catalytic activity for NH_3 synthesis, thus suggesting catalysts containing Ti and H could weaken the strong Ti-N bond.[31] As a way to explain the potential Ti-N bond weakening by Ti-H-containing catalysts, they performed DFT calculations of N_2 adsorption over the following Ti-terminated surfaces: Ti(001), TiN(111), and TiH_2(111); their results showed that indirect electronic effects from the lattice hydride were not enough to explain the activity observed. Our results above suggest that both lattice hydrides and hydride vacancies are influential in the

synthesis of NH_3 than only the mere presence of lattice hydrides in BTOH. From Figs. 5 and 7, one can see that in both the distal and alternating pathways for NH_3 synthesis, lattice hydrides provide a source of H atoms for N_2 hydrogenation and the vacancies that form as a result are imperative for the eventual cleavage of the N-N bond.

Future experimental work using inelastic neutron scattering (INS) would be necessary to identify different H species on the BTOH surface and determine which H species are consumed for hydrogenation of N_2, while quasielastic neutron scattering can be used to study dynamics of hydrides in the lattice as done recently for layered oxyhydride $SrVO_2H$.[39] Further experimental work using operando IR spectroscopy can help differentiate the two mechanisms by identifying the vibrational signatures of key intermediate structures in the alternating and distal mechanisms.

Using first principles DFT method to investigate NH_3 synthesis mechanisms over a metal catalyst supported on BTOH is also an exciting next step. An experimental study has shown that Ru, Co, or Fe loaded on a $BaTiO_{3-x}H_x$ support exhibited higher activity than the metal catalysts supported on $BaTiO_3$.[18] The study proposes that the higher activity exhibited on $Ru/BaTiO_{3-x}H_x$ was likely due to hydrogen spillover, thus preventing H_2 poisoning on Ru, while the activity of Fe or $Co/BaTiO_{3-x}H_x$ was possibly due to electron donation from H^- to Fe or Co which assists in N_2 activation. It would be interesting to verify these proposed pathways via DFT.

4. Conclusion

Using the first principles DFT method, we have investigated NH_3 synthesis pathways on the (210)-Ti_2O_2 surface termination of $BaTiO_{2.5}H_{0.5}$ (BTOH) in order to understand the role of lattice hydrides on the perovskite oxyhydride's surface chemistry. We found that N_2 prefers to adsorb on the more reduced surface Ti atom, which is bonded to a subsurface lattice hydride, while heterolytically dissociative H_2 adsorption is also facile on the surface. Then, two mechanistic hypotheses have been examined for hydrogenation of adsorbed N_2: (a) the distal pathway whereby H atoms hydrogenate N_2 to form the $*N\text{-}NH_2$ and $*N\text{-}NH_3$ key intermediates, followed by N-N bond breaking; (b) the alternating pathway whereby H atoms hydrogenate N_2 in an alternating fashion to form the intermediates such as *NHNH, before N-N bond breaking and formation of co-adsorbed $*NH/NH_2$ and $*NH_2/*NH_2$ on the surface. In the distal pathway, the subsurface

hydride vacancy from reaction of $*N_2$ with the lattice hydride was found to be key to breaking the $*N\text{-}NH_3$ bond and leading to surface nitride formation. In the alternating pathway, the neighboring surface Ti sites are key to bridging and stabilizing the *NNH intermediate. In both pathways, the hydrogenation steps are generally downhill in energy and desorption of NH_3 is the most uphill process. Our results shed light on the role of surface hydrides and their vacancies in hydrogenation of N_2 over BTOH which could be useful in understanding catalytic hydrogenation on perovskite oxyhydride in general.

Acknowledgements

This work was sponsored by the U.S. Department of Energy, Office of Science, Office of Basic Energy Sciences, Chemical Sciences, Geosciences, and Biosciences Division, Catalysis Science Program. This research used resources of the National Energy Research Scientific Computing Center, a DOE Office of Science User Facility supported by the Office of Science of the U.S. Department of Energy under contract no. DE-AC02-05CH11231.

Electronic Supplementary Information

Thermodynamic calculations; slab model; H_2 and N_2 dissociation; alternative NNH adsorption site.

References

[1] J. T. Grant, J. M. Venegas, W. P. McDermott and I. Hermans, *Chem. Rev.*, 2018, **118**, 2769-2815.
[2] J. Hwang, R. R. Rao, L. Giordano, Y. Katayama, Y. Yu and Y. Shao-Horn, *Science*, 2017, **358**, 751-756.
[3] S. Chen, T. Takata and K. Domen, *Nat. Rev. Mater.*, 2017, **2**, 17050.
[4] C. Tsounis, Y. Wang, H. Arandiyan, R. J. Wong, C. Y. Toe, R. Amal and J. Scott, *Catalysts*, 2020, **10**, 409.
[5] Y. Kobayashi, O. J. Hernandez, T. Sakaguchi, T. Yajima, T. Roisnel, Y. Tsujimoto, M. Morita, Y. Noda, Y. Mogami, A. Kitada, M. Ohkura, S. Hosokawa, Z. Li, K. Hayashi, Y. Kusano, J. Kim, N. Tsuji, A. Fujiwara, Y. Matsushita, K. Yoshimura, K. Takegoshi, M. Inoue, M. Takano and H. Kageyama, *Nat. Mater.*, 2012, **11**, 507-511.
[6] Y. Tang, Y. Kobayashi, K. Shitara, A. Konishi, A. Kuwabara, T. Nakashima, C. Tassel, T. Yamamoto and H. Kageyama, *Chem. Mater.*, 2017, **29**, 8187-8194.

[7] T. Sakaguchi, Y. Kobayashi, T. Yajima, M. Ohkura, C. Tassel, F. Takeiri, S. Mitsuoka, H. Ohkubo, T. Yamamoto, J. Kim, N. Tsuji, A. Fujihara, Y. Matsushita, J. Hester, M. Avdeev, K. Ohoyama and H. Kageyama, *Inorg. Chem.*, 2012, **51**, 11371-11376.
[8] J. F. Brice and A. Moreau, *Ann. Chim. Fr.*, 1982, **7**, 623-634.
[9] B. Huang and J. D. Corbett, *J. Solid State Chem.,* 1998, **141**, 570–575.
[10] B. Huang and J. D. Corbett, *Inorg. Chem.,* 1998, **37**, 1892–1899.
[11] M. A. Hayward, E. J. Cussen, J. B. Claridge, M. Bieringer, M. J. Rosseinsky, C. J. Kiely, S. J. Blundell, I. M. Marshall and F. L. Pratt, *Science*, 2002, 295, 1882-1884.
[12] Y. Goto, C. Tassel, Y. Noda, O. Hernandez, C. J. Pickard, M. A. Green, H. Sakaebe, N. Taguchi, Y. Uchimoto, Y. Kobayashi and H. Kageyama, *Inorg. Chem.*, 2017, **56**, 4840-4845.
[13] J. Bang, S. Matsuishi, H. Hiraka, F. Fujisaki, T. Otomo, S. Maki, J. Yamaura, R. Kumai, Y. Murakami and H. Hosono, *J. Am. Chem. Soc.*, 2014, **136**, 7221-7224.
[14] F. D. Romero, A. Leach, J. S. Möller, F. Foronda, S. J. Blundell and M. A. Hayward, *Angew. Chem. Int. Ed.*, 2014, **53**, 7556-7559.
[15] C. Tassel, Y. Goto, Y. Kuno, J. Hester, M. Green, Y. Kobayashi and H. Kageyama, *Angew. Chem.*, 2014, **126**, 10545-10548.
[16] C. Tassel, Y. Goto, D. Watabe, Y. Tang, H. Lu, Y. Kuno, F. Takeiri, T. Yamamoto, C. M. Brown, J. Hester, Y. Kobayashi and H. Kageyama, *Angew. Chem. Int. Ed.*, 2016, **55**, 9667-9670.
[17] Y. Tang, Y. Kobayashi, C. Tassel, T. Yamamoto and H. Kageyama, *Adv. Energy Mater.*, 2018, **8**, 1800800.
[18] Y. Tang, Y. Kobayashi, N. Masuda, Y. Uchida, H. Okamoto, T. Kageyama, S. Hosokawa, F. Loyer, K. Mitsuhara, K. Yamanaka, Y. Tamenori, C. Tassel, T. Yamamoto, T. Tanaka and H. Kageyama, *Adv. Energy Mater.*, 2018, **8**, 1801772.
[19] M. Appl, Ammonia, 1. Introduction, Ullmann's Encycl. Ind. Chem., 2011, DOI: 10.1002/14356007.a02_143.pub3.
[20] J. Zhang, G. Gou and B. Pan, *J. Phys. Chem. C*, 2014, **118**, 17254−17259.
[21] C. Eklöf-Österberg, R. Nedumkandathil, U. Häussermann, A. Jaworski, A. J. Pell, M. Tyagi, N. H. Jalarvo, B. Frick, A. Faraone and M. Karlsson, *J. Phys. Chem. C*, 2019, **123**, 2019−2030.
[22] Y. Kobayashi, O. Hernandez, C. Tassel and H. Kageyama, *Sci. Technol. Adv. Mater.*, 2017, **18**, 905−918.
[23] M. Kitano, J. Kujirai, K. Ogasawara, S. Matsuishi, T. Tada, H. Abe, Y. Niwa and H. Hosono, *J. Am. Chem. Soc.*, 2019, **141**, 20344−20353.
[24] G. Kresse and J. Furthmüller, *Comput. Mater. Sci.*, 1996, **6**, 15-50.
[25] G. Kresse and J. Furthmüller, *Phys. Rev. B: Condens. Matter Mater. Phys.*, 1996, **54**, 11169-11186.
[26] J. P. Perdew, K. Burke and M. Ernzerhof, *Phys. Rev. Lett.*, 1996, **77**, 3865.
[27] P. E. Blöchl, *Phys. Rev. B: Condens. Matter Mater. Phys.*, 1994, **50**, 17953-17979.
[28] S. Grimme, J. Antony, S. Ehrlich and H. Krieg, *J. Chem. Phys.*, 2010, **132**, 154104.
[29] W. Tang, E. Sanville and G. Henkelman, *J. Phys.: Condens. Matter*, 2009, **21**, 084204.
[30] K. Wang, V. Fung, Z. Wu and D.-E. Jiang, *J. Phys. Chem. C*, 2020, **124**, 18557-18563.
[31] Y. Kobayashi, Y. Tang, T. Kageyama, H. Yamashita, N. Masuda, S. Hosokawa and H. Kageyama, *J. Am. Chem. Soc.*, 2017, **139**, 18240-18246.
[32] Y. Wang, J. Cheng, M. Behtash, W. Tang, J. Luo and K. Yang, *Phys. Chem. Chem. Phys.*, 2018, **20**, 18515.
[33] H. J. Monkhorst and J. D. Pack, *Phys. Rev. B: Solid State*, 1976, **13**, 5188-5192.
[34] J. Neugebauer and M. Scheffler, *Phys. Rev. B*, 1992, **46**, 16067-16080.

[35] G. Henkelman, B. P. Uberuaga and H. Jonsson, *J. Chem. Phys.*, 2000, **113**, 9901.
[36] A. Savara, *J. Phys. Chem. C*, 2013, **117**, 15710-15715.
[37] G. Bouilly, T. Yajima, T. Terashima, W. Yoshimune, K. Nakano, C. Tassel, Y. Kususe, K. Fujita, K. Tanaka, T. Yamamoto, Y. Kobayashi and H. Kageyama, *Chem. Mater.*, 2015, **27**, 6354-6359.
[38] M. P. Shaver and M. D. Fryzuk, *Adv. Synth. Catal.*, 2003, **345**, 1061-1076.
[39] R. Lavén, U. Häussermann, A. Perrichon, M. S. Andersson, M. S. Targama, F. Demmel and M. Karlsson, *Chem. Mater.* 2021, **33**, 2967-2975.